

Let Synthetic Data Shine: Domain Reassembly and Soft-Fusion for Single Domain Generalization

Hao Li¹, Yubin Xiao^{2†}, Ke Liang¹, Mengzhu Wang¹, Long Lan¹, Kenli Li³,
Xinwang Liu¹

¹College of Computer Science and Technology, National University of Defense Technology, Changsha, 410073, China.

²College of Computer Science and Technology, Jilin University, Changchun, 130012, China.

³College of Computer Science and Electronic Engineering, Hunan University, Changsha, 410082, China.

Contributing authors: lihao96@nudt.edu.cn;

†These authors contributed equally to this work.

Abstract

Single Domain Generalization (SDG) aims to train models with consistent performance across diverse scenarios using data from a single source. While using latent diffusion models (LDMs) show promise in augmenting limited source data, we demonstrate that directly using synthetic data can be detrimental due to significant feature distribution discrepancies between synthetic and real target domains, leading to performance degradation. To address this issue, we propose Discriminative Domain Reassembly and Soft-Fusion (DRSF), a training framework leveraging synthetic data to improve model generalization. We employ LDMs to produce diverse pseudo-target domain samples and introduce two key modules to handle distribution bias. First, Discriminative Feature Decoupling and Reassembly (DFDR) module uses entropy-guided attention to recalibrate channel-level features, suppressing synthetic noise while preserving semantic consistency. Second, Multi-pseudo-domain Soft Fusion (MDSF) module uses adversarial training with latent-space feature interpolation, creating continuous feature transitions between domains. Extensive SDG experiments on object detection and semantic segmentation tasks demonstrate that DRSF achieves substantial performance gains with only marginal computational overhead. Notably, DRSF’s plug-and-play architecture enables seamless integration with unsupervised domain adaptation paradigms, underscoring its broad applicability in addressing diverse and real-world domain challenges.

Keywords: single domain generalization, synthetic data, semantic segmentation, object detection

1 Introduction

Supervised and semi-supervised deep learning methods have made significant advances in the field of computer vision (CV) [1, 2]. However,

these approaches are often based on the assumption that the training (source) and testing (target) data share the same distribution. In the presence of domain shift [3], the model’s performance in target domains can degrade sharply, severely limiting its practical applicability in real-world scenarios

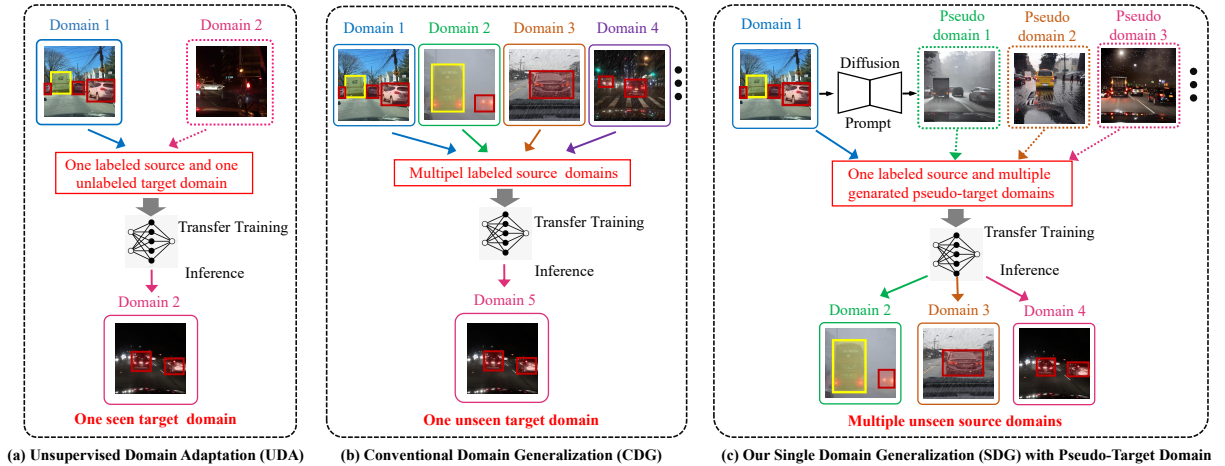


Fig. 1 A comparison of Domain Adaptation (DA), Conventional Domain Generalization (CDG), and our pseudo-target domain-based Single Domain Generalization (SDG) for object detection tasks. DA relies on aligning with target domain data (left), while CDG requires joint training across multiple source domains (middle). In contrast, our strategy only requires single-source data, using diffusion models to generate diverse pseudo-target domains (right).

[4]. To address the domain shift problem, numerous methods in Unsupervised Domain Adaptation (UDA) [5–7] and Domain Generalization (DG) [8–11] have been proposed. UDA focuses on transferring models trained on source domain to (accessible) target domains, whereas DG aims to develop models that exhibit strong cross-domain generalization capabilities across multiple (unseen) target domains. Comparing to UDA, DG emphasizes the development of plug-and-play models that can generalize effectively without the need for additional training or fine-tuning, garnering increasing attention [12]. More importantly, in real-world applications, researchers often encounter constraints related to single-source domain data (Single Domain Generalization, SDG) [13], where only data from a single source domain are accessible. This paper specifically focuses on this challenging yet realistic problem.

Existing methods in SDG primarily rely on data augmentation techniques to diversify source domain data, which has led to some progress in image classification tasks [14, 15]. However, data augmentation may introduce noise; improper enhancements may result in the loss of important image edge information, causing distortions in the target structure and deviating from the original (pre-augmentation) samples [16, 17]. This complicates the application of these methods to broader CV tasks, such as object detection. More

importantly, constrained by the limited representation of a single source domain, even enhanced data tends to cause models to overfit to the specific features of the source domain. This limits the representation of training data, makes it difficult to simulate the diversity of target domains in real-world scenarios, and ultimately reduces the generalization ability of the model [17].

Recently, generative diffusion models have become a crucial tool for enhancing model data representations due to their high fidelity and versatile cross-domain generation capabilities [18]. By leveraging these generative models to synthesize samples across different scenarios, it is possible to both mitigate the lack of diversified source domain data and expose the model to a wide range of potential target domains during training, thereby improving its generalization ability in unseen domains. Consequently, using generative models to enhance a model’s generalization has emerged as a promising approach in SDG [19]. However, existing methods primarily focus on improving the visual realism of synthetic data, often overlooking semantic consistency and distribution transferability between the synthetic domain and the real target domain. Direct application of synthetic data may fail to enhance model generalization effectively and could even lead to degeneration, which limits the practical utility of the synthetic data (see Section 3.1 for

details). Therefore, determining how to effectively utilize the synthetic data, which inherently carries distribution biases, to improve the model’s generalization ability becomes a key challenge in the field of SDG.

To address the aforementioned challenge, we propose a novel and general training framework, DRSF (Discriminative Domain Reassembly and Soft-Fusion), which utilizes synthetic data to improve generalization in SDG. We employ a generative diffusion model to produce rich and diverse target domain samples, thereby enhancing the diversity of the training data. Notably, while we also utilize synthetic data, our approach differs from existing methods by introducing two core modules designed to handle the distribution bias in synthetic data. Firstly, to mitigate the significant feature distribution gap between the synthetic pseudo-target domain data and the source domain data, which could cause model confusion during training, we propose a Discriminative Feature Decoupling and Reassembly (DFDR) module to decompose the features of both domains into primary features (domain-invariant) and shared features (domain-specific). We then reduce content discrepancy by aligning the primary features, while using the shared features to capture style variations across domains, thus enhancing the model’s cross-domain generalization ability. Secondly, to further improve the model’s adaptability to unseen target domains, we propose a Multi-Pseudo-domain Feature Soft-Fusion (MDSF) module. By blending the features of the source domain and multiple pseudo-target domains in the shared feature space, this module constructs a continuous domain-invariant feature space to smooth the boundaries between different domains and combines adversarial training to further narrow the distribution difference between the source domain and pseudo-target domain, thus fusing the decoupled features. It is important to note that, beyond SDG, we also demonstrate the extension of DRSF to UDA tasks, which further highlights the plug-and-play generality of our approach and its practical applicability to a wide range of tasks in real-world scenarios.

The key contributions of this work are as follows.

i) We demonstrate that although the synthetic data visually resembles real data, its internal distribution differs significantly, hampering the

effective enhancement of the model’s SDG generalization when using the synthetic data directly and potentially leading to localized degradation. To the best of our knowledge, our work is the first one reporting this finding in the SDG field with the support of experimental results.

ii) To effectively leverage synthetic data with inherent distributional biases, we introduce DRSF—a plug-and-play training framework designed to enhance SDG performance by decoupling and recombining features from synthetic data. To the best of our knowledge, DRSF is the first general SDG training framework that manipulates synthetic data at the feature level.

iii) We demonstrate the state-of-the-art (SOTA) generalization capabilities of DRSF in SDG tasks by conducting extensive experiments on object detection and semantic segmentation. Additionally, ablation studies validate the effectiveness of the proposed DFDR and MDSF components.

2 Related work

In this section, we first review UDA and DG methods, followed by an introduction to SDG methods applied in object detection and semantic segmentation. Finally, we present pioneering works that employ synthetic data to address SDG challenges. Additionally, we illustrate the differences between UDA, DG, and our proposed synthetic data-based method to solve SDG challenges in Fig. 1.

2.1 Unsupervised Domain Adaption and Domain Generalization

In CV tasks, models often assume that source and target domain data originate from the same distribution. However, in practical applications, significant distribution differences frequently exist between these domains, leading to substantial performance degradation on the target domain—a phenomenon known as domain shift [20]. For instance, in image classification, object detection, and semantic segmentation tasks, disparities between source and target domains may arise due to environmental factors, illumination variations, or differences in viewing angles [3, 21]. To address these challenges, UDA and DG have emerged as two pivotal techniques. UDA primarily focuses on transferring knowledge—such as content and

style—between source and target domains. In contrast, DG aims to enhance a model’s cross-domain generalization capability using only source domain data, enabling robust performance on previously unseen target domains.

Fig. 1(a) illustrates the principle of UDA, which requires access to target domain data. UDA typically employs methods such as adversarial training [22–24] and maximum mean discrepancy minimization [25] to adapt models to unlabeled data in the target domain, thereby enhancing performance. However, when the target domain distribution differs substantially from the source domain, the effectiveness of domain adaptation may be limited. Moreover, acquiring data in the target domain can be challenging or costly due to privacy concerns, expenses, or other constraints. In such cases, DG aims to train models that generalize across multiple source domains and perform well on unseen target domains. In DG, techniques like data augmentation [26–28] and meta-learning [29–32] are often utilized to learn domain-independent features, thereby mitigating overfitting to specific domains. Fig. 1(b) illustrates the principle of conventional DG methods, which often require access to multiple source domains. Notably, Zhou et al. [33] proposed a plug-and-play module named MixStyle, applicable to tasks such as UDA and DG, thereby establishing a foundational approach for effectively addressing generalization across various scenarios in related fields.

2.2 Single Domain Generalization in Object Detection and Semantic Segmentation

In DG, a particularly challenging yet practically significant task is SDG [13, 34, 35]. This task is more realistic than conventional (multi-source) DG, because many real-world applications lack access to data from multiple domains. The objective of SDG is to develop a generalized model trained on a single source domain that performs effectively across numerous unseen target domains. An intuitive approach to addressing SDG involves enhancing the diversity of single-source data through various data augmentation techniques. For instance, Carlucci et al. [36] employed a self-supervised learning strategy for data augmentation by segmenting images into

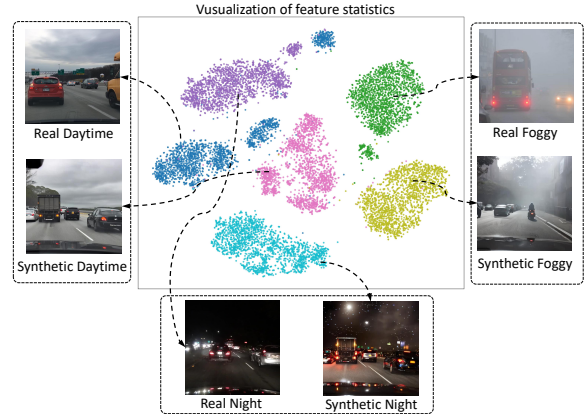


Fig. 2 2D t-SNE visualization of image feature statistics for real and diffusion-generated domains.

tiles, shuffling them, and training the model to simultaneously classify the images and predict the correct order of the shuffled tiles. Similarly, Chen et al. [37] proposed a center-aware adversarial augmentation technique that expands the source distribution by modifying source samples to distance them from class centers. Additionally, Lee et al. [38] introduced an object-aware domain generalization approach, while Vidit et al. [39] presented a novel semantic enhancement strategy utilizing a pre-trained vision-language model.

However, despite the success of data augmentation methods in image classification tasks, their adaptation to more complex computer vision tasks, such as object detection—which requires both classification and localization capabilities—remains challenging. Data augmentation in these contexts can inadvertently introduce noise, complicating model training [17]. Moreover, when only limited source domain data is available, even augmented pseudo-source domain data may lack the diversity necessary to effectively simulate real-world scenarios, because they do not incorporate knowledge beyond the original source domain.

2.3 Synthetic Data-based SDG

Recent advances in large-scale vision models underscore the potential of leveraging extensive prior knowledge embedded in foundational models pre-trained on internet-scale datasets. For instance, the C-Gap model [39] attains SOTA performance in single-domain object detection by extracting pertinent semantic information from

the CLIP model [40] using domain-specific text prompts. More recently, latent diffusion model (LDM) [41] has demonstrated a powerful ability to generate images with different styles by operating within latent spaces and incorporating text-guided techniques such as CLIP. By employing prompts and source domains to generate images across various domains, LDMs effectively simulate diversity in real-world scenarios [42, 43]. This approach mitigates the challenge of limited training data, offering a promising paradigm for generalization within a single domain.

However, our experiments reveal that while images generated directly using LDMs or existing data generation methods closely resemble real target domains visually, significant discrepancies persist in feature space. Utilizing such images without modification does not enhance, and may even impair, the model’s generalization performance (refer to Section 3.1). Consequently, the primary motivation of this study is to explore how to effectively utilize synthetic data with inherent distribution bias for SDG tasks.

3 Motivation and Problem Formulation

Generative diffusion models have emerged as a powerful tool for enhancing visual representations, owing to their high fidelity and diverse cross-domain generation capabilities. However, their application in SDG tasks still presents considerable challenges. While these models can efficiently synthesize multi-scene samples (e.g., foggy, nighttime, rainy, and snowy conditions) from a single source domain, offering new avenues for addressing data scarcity, existing research tends to overemphasize the visual realism of the synthetic data [41, 44]. This overemphasis often neglects the critical issues of semantic consistency and distribution transferability between the synthetic and real domains.

3.1 Core Challenges of Synthetic Data in Single-Domain Generalization

Data augmentation via diffusion models for SDG presents two primary challenges:

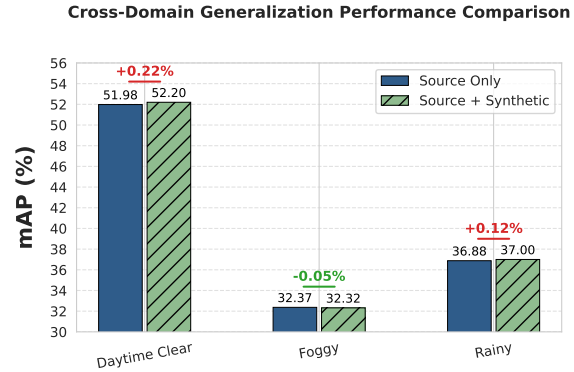


Fig. 3 Impact of the Synthetic Domain on Detector Cross-Domain Performance.

1) **Feature Space Discrepancy between Synthetic and Real Target Domains:** As illustrated in Fig. 2, despite the pixel-level similarity between diffusion-generated images and the real images, these images exhibit excessive intra-domain clustering in the feature space. While visually diverse, the synthetic samples fail to adequately represent the real target domain’s distribution, hindering the model’s ability to learn truly domain-invariant features.

2) **Artifacts and Distributional Shifts in Synthetic Data:** This discrepancy can lead the model to learn spurious artifact patterns unique to the Synthetic domain, such as non-physical fog density gradients, rather than generalizable semantic representations. Quantitative experiments using Faster R-CNN (Fig. 3) corroborate this issue: training with a direct fusion of the source domain (Daytime Clear) and diffusion-generated foggy/rainy data does not significantly improve performance on real target domains, and even degrades performance in some cases. This suggests that visual realism alone is insufficient to guarantee enhanced cross-domain generalization. Robust learning mechanisms are therefore needed to address biases introduced by synthetic data.

3.2 Formal Representation of SDG

As depicted in Fig. 1(b), CDG requires models to learn domain-invariant representations from multiple source domains. This work addresses the more challenging SDG problem. Here, the model is trained solely on data from a single source

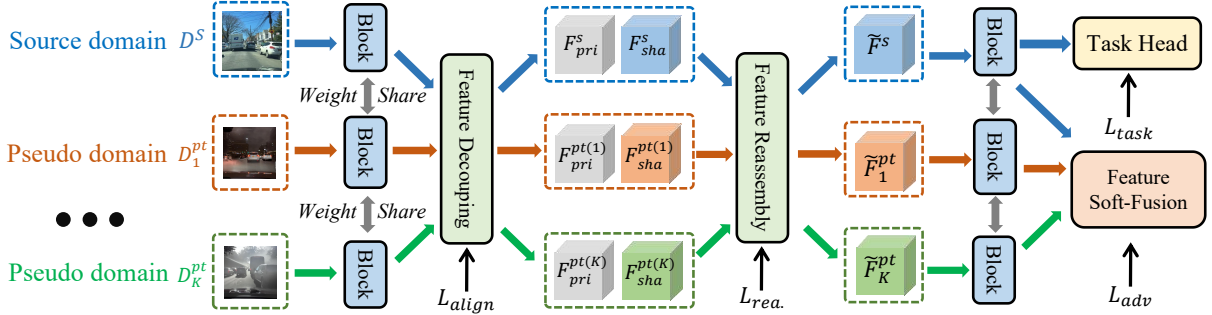


Fig. 4 The overall DRSF framework. The backbone takes diverse pseudo-target domain data $\{\mathcal{D}_i^{pt}\}_{i=1}^K$, generated from a single source domain \mathcal{D}^S , as input. These features are then decoupled into primary features (domain-invariant features) and shared features (domain-specific features). Subsequently, a feature reassembly strategy is employed to mitigate interference arising from style variations. By integrating a multi-domain feature soft-fusion strategy, a continuous cross-domain feature space is constructed. The feature decoupling reassembly is embedded within the backbone network blocks, while the feature soft-fusion processes the output features from the backbone.

domain, \mathcal{D}^s , and must generalize to T unseen target domains, $\{\mathcal{D}_j^t\}_{j=1}^T$. Each target domain \mathcal{D}^t follows an unknown distribution $\mathcal{P}_t(\mathbf{x}, \mathbf{y})$, where $\mathcal{P}_t \neq \mathcal{P}_s$. The objective of SDG is to learn a parameterized mapping $f_\theta : \mathcal{X} \rightarrow \mathcal{Y}$ that minimizes the risk function on the target domain:

$$\mathcal{R}_t(f_\theta) = \mathbb{E}_{(\mathbf{x}, \mathbf{y}) \sim \mathcal{P}_t} [\mathcal{L}(f_\theta(\mathbf{x}), \mathbf{y})], \quad (1)$$

where $\mathcal{L}(\cdot)$ denotes the task-specific loss function. Given that the target domain distribution \mathcal{P}_t is inaccessible during training, the central challenge of SDG is to construct a sufficiently broad representation space from a single source distribution, enabling effective handling of potential domain shifts. Inspired by Ben-David et al.’s domain adaptation theory [5], we recognize that the upper bound of the target domain error is related to both the source domain error and the domain discrepancy. Our key insight is that *constructing a series of pseudo-target domains and establishing a continuous transition manifold in feature space can reduce the model’s expected risk on unseen target domains*. As illustrated in Fig. 1(c), we specifically construct multiple pseudo-target domain distributions, $\{\mathcal{P}_{pt}^i\}_{i=1}^K$, to approximate potential target domains, and formulate a proxy optimization objective:

$$\min_{\theta} \left\{ \frac{1}{K} \sum_{i=1}^K \mathbb{E}_{(\mathbf{x}, \mathbf{y}) \sim \mathcal{P}_{pt}^i} [\mathcal{L}(f_\theta(\mathbf{x}), \mathbf{y})] + \lambda \cdot \frac{1}{K} \sum_{i=1}^K \mathcal{D}_\phi(\mathcal{P}_s, \mathcal{P}_{pt}^i) \right\}, \quad (2)$$

where $\mathcal{D}_\phi(\cdot)$ symbolizes a parameterized generalization model to create a structured mapping in the source domain and several pseudo-target domains. Rather than merely considering mappings between individual domain pairs, this model establishes a continuous feature transformation space, effectively covering paths from the source domain to various potential target domains. Parameter λ balances between DG and downstream task learning. Instead, we strive to build a feature space that is continuous and sufficiently broad and invariant to domains. Any unseen target domain should get approximately represented by the manifold of this feature space. Thus, covering distribution space allows the model to learn rich domain shift patterns and gain better generalization performance in unseen environments.

4 Method

4.1 overview

To overcome the challenges of SDG and fully exploit synthetic data, we introduce Domain Reassembly and Soft-Fusion (DRSF), a novel

unified SDG method. As illustrated in Fig. 4, DRSF adopts a four-stage collaborative learning paradigm - generation, decoupling, reassembly, and fusion - to maximize the utility of synthetic data:

1) **Pseudo-target domain generation:** We leverage diffusion models to synthesize pseudo-target domain data with diverse stylistic variations. While preserving the semantic structure of the source domain \mathcal{D}^S , this process simulates domain shifts across different environmental conditions. Although this expands training data diversity, synthetic data still suffers from feature space bias and artifact patterns as analyzed in Section 3.1;

2) **Discriminative Feature Decoupling and Reassembly (DFDR):** To mitigate limitations of synthetic data, we propose an embedded DFDR module within the backbone network. This decomposes features into primary features (domain-invariant) and shared features (domain-specific). By employing entropy-guided channel attention mechanisms, we selectively amplify synergistic channels while suppressing noisy ones. This dual process reduces artifact interference in synthetic data while strengthening cross-domain discriminative capabilities;

3) **Multi-Pseudo-domain Feature Soft-Fusion (MDSF):** The MDSF module establishes smooth feature transitions between the source domain and multiple pseudo-target domains using soft label assignments and linear interpolation. Combined with adversarial training, this enables the model to learn domain-invariant representations that effectively cover the distribution space of potential target domains.

Unlike conventional approaches focusing solely on visual realism [41, 45], DRSF addresses feature space biases through structural feature reassembly and continuous fusion. This turns synthetic data into useful tools that improve generalization. The framework’s modular design allows seamless integration with existing UDA methods, making it broadly applicable beyond single-domain scenarios.

4.2 Pseudo-target Domain Generation

In this section, we describe how LDMs are employed to generate pseudo-target domains that

maintain semantic consistency while introducing stylistic diversity. This serves as the foundation for subsequent feature decoupling and fusion steps. The key advantages of using diffusion models for pseudo-target domain generation include: 1) Pixel-level fine-tuning is enabled through a combination of forward noise addition and gradual denoising processes; 2) Compared to GAN [46] and VAE [47], diffusion models offer more stable style transformations without compromising semantic consistency; 3) They support a variety of conditional constraints to ensure high-quality generation. For our specific implementation, we utilize InstanceDiffusion [44], which leverages instance-level control to apply distinct style transformations to different objects within an image. This approach maximizes domain diversity while ensuring structural integrity is preserved.

As illustrated in Figure 1(c), starting from a source domain dataset $\mathcal{D}^s = \{(\mathbf{x}_i^s, \mathbf{y}_i^s)\}_{i=1}^{N_s}$, we proceed to construct pseudo-target domain images:

$$\mathbf{x}_i^{pt} = \mathcal{F}(\mathbf{x}_i^s, P^{pt}, C(\mathbf{x}_i^s)), \quad (3)$$

where \mathcal{F} denotes the diffusion model, P^{pt} represents the prompt for the target domain (e.g., “nighttime foggy city street scene”), and $C(\cdot)$ imposes structural constraints (e.g., bounding box locations, edges). In the context of object detection, $\mathbf{y}_i^s = \{\mathbf{c}_j, \mathbf{b}_j\}_{j=1}^{N_b}$ comprises object categories \mathbf{c}_j and bounding box coordinates $\mathbf{b}_j \in \mathbb{R}^4$.

To address the nuances of various visual tasks, we have tailored specific generative strategies:

- **Semantic Segmentation:** We present a special style prompting [45] approach that involves using weather condition labels in conjunction with topological ground structure priors. While transferring the domain styles, this approach guarantees that the semantic boundaries are preserved impeccably in the synthetic images.
- **Object Detection:** A dual-prompting mechanism is utilized here. We first use a global environmental transformation [48] on the whole image, like changing an urban background into a snowy night scene. Then, a fine-grained stylistic alteration is applied to the object regions, such as transforming the car into a vintage model, thus enabling precise style manipulation at the object level.

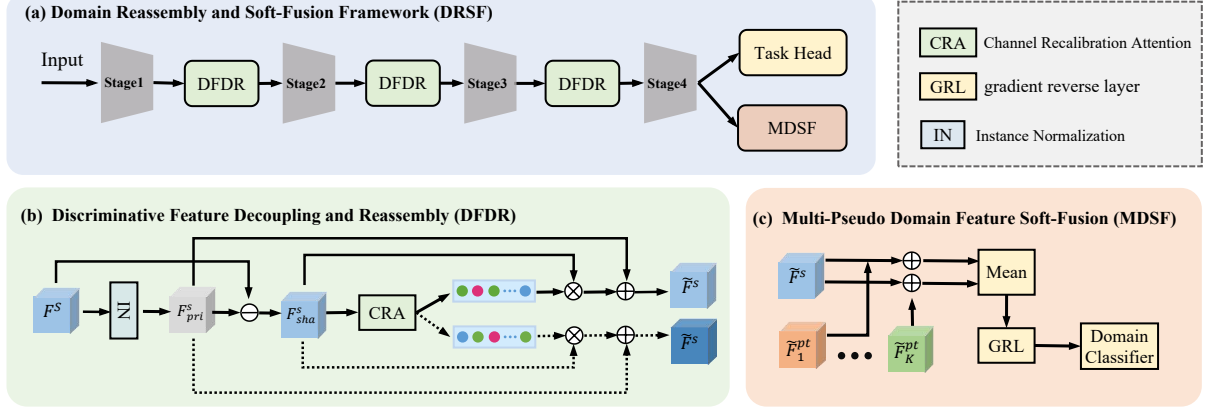


Fig. 5 (a) Illustration of the DRSF framework, where the DFDR module is embedded within the blocks of the backbone network, and the MDSF operates on the backbone’s output. (b) Example diagram of the proposed DFDR. This module employs Instance Normalization (IN) to decompose intermediate features, followed by channel recalibration attention for feature reassembly. This feature reassembly strategy reduces interference arising from style variations. (c) The proposed MDSF. This module aims to achieve smooth fusion between the source and pseudo-target domains at the feature level through linear interpolation, thereby constructing a continuous cross-domain feature space.

Following the strategy above, we construct K distinct pseudo-target domain datasets, denoted as $\{\mathcal{D}_i^{pt}\}_{i=1}^K$. To address the key challenge of single-domain generalization when using synthetic data, the following sections will detail how we leverage the potential drawbacks of these pseudo-target domains to instead improve the model’s generalization performance.

4.3 Discriminative Feature Decoupling and Reassembly

This section introduces the Discriminative Feature Decoupling and Reassembly (DFDR) module. As illustrated in Fig. 5(a), DFDR is embedded within the backbone network layers to process features.

To handle the features of the synthetic pseudo-domain data, we utilize Instance Normalization (IN) for feature decoupling. Originally introduced by Ulyanov et al. [49] for style transfer, IN normalizes the features of each sample independently, effectively removing sample-specific style variations. Specifically, IN computes statistics for each instance across the spatial dimensions:

$$\mu_{nc}(F) = \frac{1}{HW} \sum_{h,w} F_{nchw}, \quad (4)$$

$$\sigma_{nc}(F) = \sqrt{\frac{1}{HW} \sum_{h,w} (F_{nchw} - \mu_{nc}(F))^2}. \quad (5)$$

IN effectively disentangles content and style representations [50], enabling the distinction between structural information and stylistic noise in diffusion-generated images. This allows models to focus on learning domain-invariant features. Li et al. [51] further showed that IN implicitly performs style normalization in neural feature spaces, separating content and style into distinct channel-based representations. Motivated by this theoretical basis and practical requirements, we developed an IN-based feature decoupling mechanism for synthetic data. This mechanism explicitly partitions features into domain-invariant primary features (capturing task-relevant structural information) and domain-specific shared features (encoding style variations), simultaneously addressing pseudo-domain feature biases and establishing a structural framework for subsequent reassembly.

As shown in Fig. 5(b), the internal architecture of DFDR begins by decomposing the intermediate features $F \in \mathbb{R}^{N \times C \times H \times W}$ (with N denoting batch size, C channel count, H spatial height, and W spatial width) extracted from the backbone network into two distinct components:

$$F_{pri} = \gamma \odot \frac{F - \mu(F)}{\sigma(F)} + \beta, \quad (6)$$

$$F_{sha} = F - F_{pri},$$

Specifically, F_{pri} corresponds to domain-invariant primary features that encode task-relevant structural information, while F_{sha} captures domain-specific shared features encompassing style and appearance variations. The affine parameters γ and β are learnable, and $\mu(F) \in \mathbb{R}^{N \times C}$ and $\sigma(F) \in \mathbb{R}^{N \times C}$ denote the spatially aggregated mean and standard deviation of the features, respectively.

We concurrently apply the decoupling process to features from the source domain and K pseudo target domains, deriving a single set of domain-decoupled source features and K corresponding sets for the pseudo target domains respectively:

$$\{F_{pri}^s, F_{sha}^s\}, \{F_{pri}^{pt(i)}, F_{sha}^{pt(i)}\}_{i=1}^K.$$

To enforce domain-invariant consistency in primary features, we employ the Maximum Mean Discrepancy (MMD) [52] loss to align the source domain’s features with those of the pseudo target domains, ensuring cross-domain structural alignment.

$$\mathcal{L}_{\text{align}} = \frac{1}{K} \sum_{k=1}^K \text{MMD}(F_{pri}^s, F_{pri}^{pt(i)}), \quad (7)$$

By suppressing noise in synthetic imagery, this alignment mechanism fosters the development of robust domain-invariant feature representations within the latent space.

4.3.1 Feature Reassembly

While retaining primary features risks discarding valuable discriminative signals, shared features often encapsulate both informative and disruptive components. To balance noise suppression and discriminative channel utilization, we propose a *style-recalibrated feature reassembly framework*. At its core lies the **Channel Recalibration Attention (CRA)**, which performs fine-grained selection of salient features within shared channels. Unlike conventional attention schemes [53, 54], our approach explicitly identifies “gain” and “interference” channels during training by analyzing the entropy of the network’s feature input responses.

The process begins with extracting style representations of shared features via global statistical modeling:

$$Q_{n,c} = [\mu_{n,c}(F_{sha}) \parallel \sigma_{n,c}(F_{sha})], \quad (8)$$

Here, $Q \in \mathbb{R}^{N \times C \times 2}$ encodes the global statistics $\mu_{n,c}$ (mean) and $\sigma_{n,c}$ (standard deviation) for the c -th channel of the n -th sample. Following this, we perform channel-wise linear transformations and batch normalization to refine the feature representations:

$$T_{n,c} = W_c \cdot Q_{n,c}, \quad (9)$$

$$\hat{T}_{n,c} = \gamma_c \frac{T_{n,c} - \mu_c^{(T)}}{\sigma_c^{(T)}} + \beta_c, \quad (10)$$

where $\mu_c^{(T)}$ and $\sigma_c^{(T)}$ represent the mean and standard deviation computed across the batch dimension, while γ_c and β_c denote learnable parameters. To obtain the channel-wise attention weights, we apply the Sigmoid function as follows:

$$V_{n,c} = \sigma(\hat{T}_{n,c}) = \frac{1}{1 + e^{-\hat{T}_{n,c}}}. \quad (11)$$

This yields an attention vector $V \in \mathbb{R}^{N \times C}$, where each element quantifies a channel’s contribution to the discriminative task. Specifically, V^s and V^{pt} correspond to the channel recalibration attention vectors for the source domain and pseudo-target domain, respectively.

Feature Reassembly

To process the source domain’s shared features F_{sha}^s , we employ the CRA attention vector V^s to perform channel-wise fusion with primary features F_{pri}^s , generating two complementary residual components:

$$\begin{aligned} \tilde{F}^s &= F_{pri}^s + V^s \odot F_{sha}^s, \\ \hat{F}^s &= F_{pri}^s + (1 - V^s) \odot F_{sha}^s. \end{aligned} \quad (12)$$

The \tilde{F}^s emphasizes cooperative gain features by prioritizing high-attention channels, while \hat{F}^s isolates interference features from low-attention channels. This dual decomposition enables distinct treatment of beneficial and detrimental channels during discriminative processing.

Entropy Difference Supervision.

To steer the optimization of feature reassembly, we propose a loss function based on predictive

entropy differences:

$$\begin{aligned} \mathcal{L}_{\text{rea}} = & \text{ReLu}^+(H(\phi(\tilde{F}^s)) - H(\phi(F_{pri}^s))) \\ & + \text{ReLu}^+(H(\phi(F_{pri}^s)) - H(\phi(\hat{F}^s))), \end{aligned} \quad (13)$$

where $H(\phi(F)) = -\sum_{k=1}^{N_K} p_k(F) \log p_k(F)$ quantifies the predictive entropy derived from feature F , with ϕ being the task-specific prediction head and $p_k(F)$ denoting the predicted probability for class k . The $\text{ReLu}^+(x) = \ln(1 + e^x)$ operator smooths the regularization constraint. By comparing predictive entropies, this loss function promotes features that reduce uncertainty through synergistic interactions, while penalizing channels that introduce ambiguity. This entropy-driven supervision mechanism aligns with the feature space bias analysis in Section 3.1, thereby improving the utility of synthetic data during training.

4.4 Multi-Pseudo Domain-Based Feature Soft Fusion Training Framework

To establish a smoother cross-domain feature transformation space, this work introduces the Multi-Pseudo Domain Soft Fusion (MDSF) module (Fig. 5(c)). By integrating feature-level interpolation and adversarial training, MDSF constructs a continuous feature space across multiple discrete pseudo-domains while learning domain-invariant discriminative representations.

4.4.1 Multi-Pseudo Domain Soft Fusion

In contrast to conventional input-space mixing that risks semantic distortion [55], MDSF performs feature-level fusion on structured features from the DFDR module. This approach ensures precise integration as follows: First, we extract reassembled features from the k -th pseudo-target domain, then blend them with source-domain primary features to form a unified representation.

$$\tilde{F}_i^{pt} = F_{pri}^{pt(i)} + V^{pt} \odot F_{sha}^{pt(i)}, \quad (14)$$

$$F_i^{sf} = \lambda F_{pri}^s + (1 - \lambda) \tilde{F}_i^{pt}. \quad (15)$$

The mixing coefficient λ is sampled from a symmetric beta distribution $\text{Beta}(\alpha_1, \alpha_2)$ with

$\alpha_1 = \alpha_2$, where $\alpha = 2.0$ ensures a balanced sampling distribution. This feature-level interpolation constructs a continuous feature path from the source domain to the i -th pseudo-target domain. To synchronize domain label consistency with feature blending, we apply corresponding label interpolation in parallel:

$$L_i^{sf} = \lambda L^s + (1 - \lambda) L_i^{pt}, \quad (16)$$

where L^s and L_i^{pt} denote the domain labels for the source and pseudo-target domains, respectively. By employing soft labels, the adversarial training achieves smoother gradient distributions, thereby circumventing domain boundary conflicts that hard labels might induce.

Aiming to broaden domain coverage and mitigate domain-specific noise from individual pseudo domains, we average all interpolated features across source-pseudo domain pairs:

$$\tilde{F}^{sf} = \frac{1}{K} \sum_{i=1}^K F_i^{sf}. \quad (17)$$

This approach effectively constructs a feature space centered at the source domain and radiating towards multiple pseudo-target domains. The corresponding domain labels are fused using the same strategy:

$$\tilde{L}^{sf} = \frac{1}{K} \sum_{i=1}^K L_i^{sf}. \quad (18)$$

4.4.2 Adversarial Training

To further encourage learning of domain-invariant discriminative features, we employ a GRL-based adversarial training framework [56]. A domain classifier D is designed to discriminate between source domain features, pseudo-target domain features, and their fused counterparts, while adversarial optimization eliminates domain-specific information through opposing objectives:

$$\begin{aligned} \mathcal{L}_{adv} = & \mathcal{L}_{\text{CE}}(D(\tilde{F}^s), L^s) \\ & + \frac{1}{K} \sum_{i=1}^K \mathcal{L}_{\text{CE}}(D(\tilde{F}_i^{pt}), L_i^{pt}) \\ & + \mathcal{L}_{\text{CE}}(D(\tilde{F}^{sf}), \tilde{L}^{sf}), \end{aligned} \quad (19)$$

where \mathcal{L}_{CE} represents the cross-entropy loss. In this adversarial framework, the domain classifier D strives to distinguish features across domains, while the feature extractor learns domain-invariant representations via GRL. This dual process forces the model to prioritize cross-domain discriminative patterns while suppressing domain-specific noise. The MDSF module synergizes with the DFDR module: DFDR improves intra-domain feature quality through decoupling, whereas MDSF constructs a continuous cross-domain feature manifold. Together, they address the two critical challenges outlined in Sections 3.1, thereby significantly boosting the model’s domain generalization performance.

4.5 Joint Optimization Objective

Building upon the DFDR and MDSF modules described earlier, we formulate a comprehensive optimization objective that balances task performance, feature quality, and domain generalization capabilities. Our total loss function is defined as:

$$\mathcal{L}_{\text{total}} = \mathcal{L}_{\text{task}} + \lambda_1 \mathcal{L}_{\text{align}} + \lambda_2 \mathcal{L}_{\text{rea.}} + \lambda_3 \mathcal{L}_{\text{adv}}, \quad (20)$$

Here, $\mathcal{L}_{\text{task}}$ represents the downstream task-specific losses, such as detection classification/regression or segmentation pixel-wise cross-entropy, which ensure that the model has a discriminative foundation. $\mathcal{L}_{\text{align}}$ (Eq. 7) measures the domain feature distribution gap via MMD between the source and pseudo-target domains to foster cross-domain alignment. On the other hand, \mathcal{L}_{adv} (Eq. 19) comes from adversarial domain classification in MDSF to encourage domain-invariant feature learning for robust generalization. Furthermore, $\mathcal{L}_{\text{rea.}}$ invokes DFDR’s entropy difference regularization in 13 to reinforce salient feature channels while suppressing noise, thus enhancing feature discriminability. These will be controlled by the hyperparameters $\lambda_1, \lambda_2, \lambda_3$, which will trade off these complementary objectives.

4.6 Application and Extension

During training, the model ingests both the source domain and multiple pseudo-target domains. The DFDR module refines intermediate features extracted by the backbone, while the MDSF module performs soft fusion. A joint optimization

strategy then updates the backbone, DFDR module, task-specific head, and domain classifier until convergence is achieved. In contrast, the inference phase is streamlined, retaining only the backbone and DFDR module. Test images are processed to yield enhanced features \tilde{F}^t , which are directly fed into the task-specific head for prediction. The MDSF module and interference pathways are deactivated during inference, minimizing computational overhead and ensuring efficient deployment.

4.6.1 Task-specific Implementation

The DFDR and MDSF modules are designed to flexibly accommodate diverse visual tasks, with their primary distinction lying in entropy metric computation strategies:

Object Detection For detection architectures, the DFDR module is embedded within the backbone network to assess entropy differences at the region level. Specifically, classification entropy is calculated for each Region of Interest (RoI) feature. The effectiveness of feature selection is evaluated using the average entropy across all foreground RoIs. In two-stage detectors such as Faster R-CNN [2], entropy computation occurs post RoI Pooling; for single-stage frameworks [57], calculations are performed at foreground locations within feature maps.

Semantic Segmentation In segmentation tasks, pixel-level entropy differences are computed. Our approach calculates prediction entropy at every spatial location in the decoder’s output, then averages these values across the entire feature map to derive a global entropy measure. This is formalized as:

$$H(\phi(F)) = -\frac{1}{HW} \sum_{h=1}^H \sum_{w=1}^W \sum_{k=1}^{N_K} p_{k,h,w}(F) \log p_{k,h,w}(F), \quad (21)$$

where $p_{k,h,w}(F)$ represents the predicted probability of the pixel at coordinate (h, w) belonging to class k .

4.6.2 Integration with UDA Methods

The proposed method functions as a plug-and-play component that seamlessly integrates with

Table 1 Performance comparison with state-of-the-art methods under different weather conditions.

Method	Venue	Daytime Clear	Night Sunny	Dusk Rainy	Night Rainy	Daytime Foggy	mPT (%) \uparrow
F-RCNN [2]	NeurIPS (2015)	50.2	31.2	26.0	12.1	32.0	25.3
SW [58]	ICCV (2019)	50.6	33.4	26.3	13.7	30.8	26.1
IBN-Net [59]	ECCV (2018)	49.7	32.1	26.1	14.3	29.6	25.5
IterNorm [60]	CVPR (2019)	43.9	29.6	22.8	12.6	28.4	23.4
ISW [61]	CVPR (2021)	51.3	33.2	25.9	14.1	31.8	26.0
S-DGOD [62]	CVPR (2022)	<u>56.1</u>	36.6	28.2	16.6	33.5	28.7
C-Gap [39]	CVPR (2023)	51.3	36.9	32.3	18.7	38.5	31.6
SRCD [63]	TNNLS (2024)	-	36.7	28.8	17.0	35.9	29.6
SHADE [64]	IJCV (2024)	-	33.9	29.5	16.8	33.4	28.4
Li et al. [43]	CVPR (2024)	53.6	38.5	33.7	<u>19.2</u>	39.1	<u>32.6</u>
OA-DG [38]	AAAI (2024)	55.8	38.0	<u>33.9</u>	16.8	38.3	31.8
Ours	-	57.7	40.2	39.8	20.2	<u>38.6</u>	34.7

UDA techniques, establishing an integrated framework with generation augmentation, feature optimization, and domain adaptation capabilities. This is implemented through:

$$\min_{\theta} \left(\mathcal{L}_{\text{total}}(\mathcal{D}^s; \theta) + L_{\text{uda}}(\mathcal{D}^s, \{\mathcal{D}_i^{pt}\}_{i=1}^K; \theta) \right), \quad (22)$$

where $\mathcal{L}_{\text{total}}$ represents the combined loss from Eq. (20), while L_{uda} encapsulates domain alignment or self-supervised objectives specific to UDA. The pseudo-target domain datasets $\{\mathcal{D}_i^{pt}\}_{i=1}^K$, functioning as either substitutes or complementary data to the target domain, substantially enhance the diversity coverage of target domain variations.

5 Experiments

This section validates the effectiveness of our DRSF framework through two fundamental vision tasks: object detection and semantic segmentation. We conduct comprehensive comparisons with state-of-the-art SDG methods, perform component-wise ablation studies, analyze detection performance, and present visual interpretations.

5.1 Single-Domain Generalization for Object Detection (SDG-OD)

5.1.1 Experimental Setup

Datasets The experiments utilize the Diverse Weather Dataset (DWD)[62], a benchmark

for evaluating SDG in object detection. This dataset encompasses five weather conditions for autonomous driving scenarios: Daytime-Clear, Night-Clear, Night-Rainy, Dusk-Rainy, and Daytime-Foggy. The Daytime-Clear subset contains 27,708 images (19,395 for training, 8,313 for testing). Night-Sunny includes 26,158 images. The rain-based scenes (Dusk-Rainy and Night-Rainy) were synthetically generated from BDD-100k [65] images, yielding 3,501 and 2,494 images respectively. The foggy scenario includes 3,775 images. All datasets share seven common object categories: bus, bike, car, motor, person, rider, and truck. For fair UDA comparisons, we also incorporate Cityscapes [66] and FoggyCityscapes [67] datasets.

Implementation Details and Evaluation

Metrics In our experimental protocol, we consider only Daytime-Clear training data as the only source domain, keeping other conditions for testing. To create pseudo target domains, we adapt the InstanceDiffusion model [44] according to the proposed method in Section 4.2 for generating 11,233 images across five virtual scenarios: Virtual Daytime, Night, Foggy, Rainy, and Dusk. The MIC framework [68] will be our default UDA component. All detection experiments are conducted in a Faster R-CNN [2] architecture with a ResNet-101 backbone [69] and stochastic gradient descent optimally trained with a 0.01 initial learning rate (batch size 8, 36K iterations) and step decay at 24K/32K iterations. Training is performed on four

Table 2 Per-class results (%) for Daytime Foggy and Dusk Rainy conditions.

Method	Daytime Foggy								Dusk Rainy							
	Bus	Bike	Car	Mot.	Pers.	Rider	Truck	mAP	Bus	Bike	Car	Mot.	Pers.	Rider	Truck	mAP
F-RCNN [2]	30.7	26.7	49.7	26.2	30.9	35.5	23.2	31.9	36.8	15.8	50.1	12.8	18.9	12.4	39.5	26.6
SW [58]	30.6	26.2	44.6	25.1	30.7	34.6	23.6	35.2	38.8	16.7	50.1	10.4	20.1	13.0	38.8	26.3
IBN-Net [59]	29.9	26.1	44.5	24.4	26.2	33.5	22.4	29.6	37.0	14.8	50.3	11.4	17.3	13.3	38.4	26.1
IterNorm [60]	29.7	21.8	42.4	24.4	26.0	33.3	21.6	28.5	32.9	14.1	38.9	11.0	15.5	11.6	35.7	22.8
ISW [61]	29.5	26.4	49.2	27.9	30.7	34.8	24.0	31.8	34.7	16.0	50.0	11.1	17.8	12.6	38.8	25.9
S-DGOD [62]	32.9	28.0	48.8	29.8	32.5	38.2	24.1	33.5	37.1	19.6	50.9	13.4	19.7	16.3	40.7	28.2
SRCD [63]	36.4	30.1	52.4	31.8	33.4	40.1	27.7	35.9	<u>39.5</u>	21.4	50.6	11.9	20.1	<u>17.6</u>	40.5	28.8
C-Gap [39]	36.1	<u>34.3</u>	58.0	33.1	39.0	<u>43.9</u>	25.1	38.5	37.8	22.8	60.7	<u>16.8</u>	26.8	18.7	42.4	32.3
Li et al. [43]	<u>36.1</u>	34.5	<u>58.4</u>	<u>33.3</u>	<u>40.5</u>	44.2	<u>26.2</u>	39.1	39.4	<u>25.2</u>	<u>60.9</u>	20.4	<u>29.9</u>	16.5	<u>43.9</u>	<u>33.7</u>
Ours	35.4	32.9	61.1	34.2	41.1	42.8	22.7	<u>38.6</u>	47.5	30.6	70.6	14.6	39.4	28.6	47.7	39.8

Table 3 Per-class results (%) for Night Sunny and Night Rainy.

Method	Night Sunny								Night Rainy							
	Bus	Bike	Car	Mot.	Pers.	Rider	Truck	mAP	Bus	Bike	Car	Mot.	Pers.	Rider	Truck	mAP
F-RCNN [2]	37.7	30.6	49.5	15.4	31.5	28.6	40.8	33.5	22.6	11.5	27.7	0.4	10.0	10.5	19.0	14.5
SW [58]	38.7	29.2	49.8	16.6	31.5	28.0	40.2	33.4	22.3	7.8	27.6	0.2	10.3	10.0	17.7	13.7
IBN-Net [59]	37.8	27.3	49.6	15.1	29.2	27.1	38.9	32.1	24.6	10.0	28.4	0.9	8.3	9.8	18.1	14.3
IterNorm [60]	38.5	23.5	38.9	15.8	26.6	25.9	38.1	29.6	21.4	6.7	22.0	0.9	9.1	10.6	17.6	12.6
ISW [61]	38.5	28.5	49.6	15.4	31.9	27.5	41.3	33.2	22.5	11.4	26.9	0.4	9.9	9.8	17.5	14.1
S-DGOD [62]	40.6	<u>35.1</u>	50.7	19.7	34.7	32.1	<u>43.4</u>	36.6	24.4	11.6	29.5	<u>9.8</u>	10.5	11.4	19.2	16.6
SRCD [63]	43.1	32.5	52.3	<u>20.1</u>	34.8	<u>31.5</u>	42.9	36.7	26.5	<u>12.9</u>	32.4	0.8	10.2	<u>12.5</u>	<u>24.0</u>	17.0
C-Gap [39]	37.7	34.3	58.0	19.2	37.6	28.5	42.9	36.9	28.6	12.1	<u>36.1</u>	9.2	12.3	9.6	22.9	18.7
Li et al. [43]	<u>40.9</u>	35.0	<u>59.0</u>	21.3	<u>40.4</u>	29.9	42.9	<u>38.5</u>	25.6	12.1	35.8	10.1	<u>14.2</u>	12.9	22.9	<u>19.2</u>
Ours	41.9	38.3	65.2	16.4	43.9	30.7	45.3	40.2	<u>28.4</u>	13.4	41.9	2.2	18.0	11.5	25.7	20.2

RTX 3090 GPUs. According to standard evaluation protocols [62], mean Average Precision mAP@0.5 is reported, and the mean Performance across Target domains mPT is computed for a comprehensive assessment.

5.1.2 Comparison with State-of-the-Art SDG-Methods

Overall SDG-OD Results Table 1 presents a performance comparison of our method against state-of-the-art SDG-OD methods across target domains. Our method achieves an mPT of 34.7%, outperforming the previous best method [43] (32.6%), thus demonstrating its effectiveness. Notably, performance on the source domain improves by 7.4%, indicating that our pseudo-target domain generation technique not only bolsters model generalization but also enhances fundamental discriminative capabilities. Visual results in Fig. 6 illustrate the performance of both the baseline and our model across complex scenarios. Compared to baseline methods, our approach achieves more accurate object localization and classification across diverse weather conditions.

Daytime-Clear to Daytime-Foggy Scene

In addressing the domain shift from clear to foggy conditions, the left half of Table 2 provides a category-wise performance analysis. Our method achieves an mAP of 38.6%, significantly outperforming the SRCD (35.9%). Notably, in the severely fog-affected ‘‘Car’’ category, our approach attains 61.1% AP, demonstrating the efficacy of our DFDR module in mitigating feature degradation caused by low-contrast fog. The strong performance (41.1% AP) in ‘‘Person’’ detection highlights our method’s ability to preserve fine-grained discriminative features.

Daytime-Clear to Dusk-Rainy Scene

For the challenging Dusk-Rainy scenario characterized by light attenuation and precipitation, results in Table 2 (right) show our method achieves an mAP of 39.8%, outperforming competing approaches. This validates our soft feature fusion strategy’s capability to handle compound domain shifts. In critical categories like ‘‘Car’’ (70.6% mAP) and ‘‘Person’’ (39.4% mAP), we establish new performance benchmarks. For the rain-sensitive ‘‘Bike’’ class, our 30.6% mAP represents an 11.0%

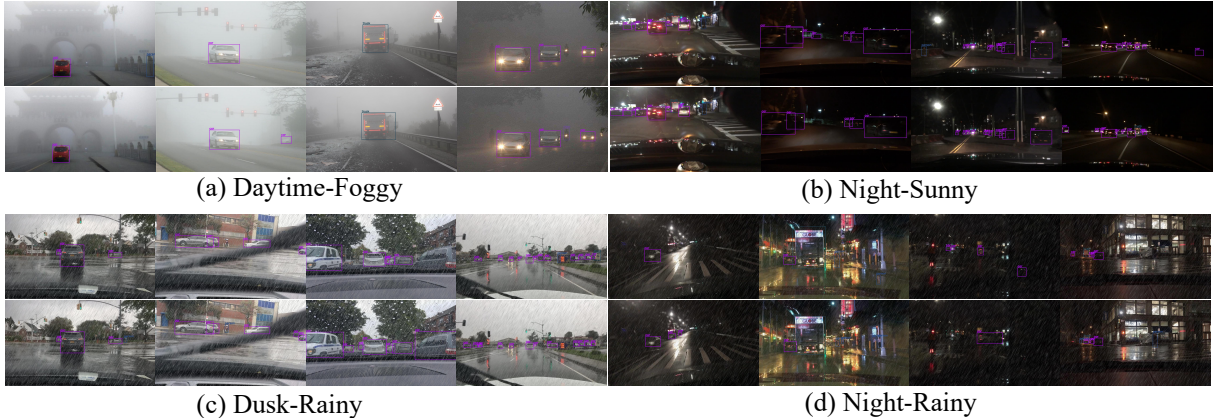


Fig. 6 Qualitative comparison of object detection results between the baseline (vanilla Faster R-CNN, top row) and our method (bottom row) across diverse weather domains. Our method demonstrates improved accuracy compared to the baseline.

improvement over S-DGOD, showcasing the synergy between DRSF mechanisms in complex environments.

Daytime-Clear to Night-Sunny Scene

The left half of Table 3 shows our method achieves an mAP of 40.2%, surpassing Li et al.’s approach [43] (38.5%) and S-DGOD (36.6%). In nighttime scenarios, our method’s generation of realistic headlight reflection features through diffusion models yields a record 65.2% mAP in “Car” detection. For “Person” detection, our 43.9% mAP exceeds PODL by 3.5%, addressing contour ambiguity under low-light conditions through enhanced feature robustness.

Daytime-Clear to Night-Rainy Scene In the most challenging Night-Rainy scenario (Table 3 right), our method maintains robustness with 20.2% mAP. The 41.9% car AP demonstrates effective noise suppression through multi pseudo domain feature fusion. While motorbike detection remains challenging (2.2% AP), our approach shows 4.5 \times improvement over F-RCNN. Current limitations in rider detection (9.1% AP) suggest future directions for disentangling precipitation artifacts from human textures. Nevertheless, our framework consistently outperforms competitors across 5/7 categories, confirming its practical value in extreme conditions.

Table 4 Performance comparison with state-of-the-art methods on SDG-SS using ResNet-101. Models were trained on GTA5 and evaluated on Cityscapes, BDD100k, and Mapillary Vistas.

Method	Venue	CS	BDD	MV	Avg.
IBN-Net [59]	ECCV 18	37.37	34.21	36.81	36.13
ISW [61]	CVPR 21	37.20	33.36	35.57	35.38
GTR* [70]	TIP 21	43.70	39.60	39.10	40.80
SAN-SAW [71]	CVPR 22	45.33	41.18	40.77	42.43
FSDR [72]	CVPR 21	44.80	41.20	43.40	43.13
AdvStyle [73]	NeurIPS 22	44.51	39.27	43.48	42.42
WildNet* [74]	CVPR 22	45.79	41.73	47.08	44.87
WEDGE* [75]	ICRA 23	45.18	41.06	48.06	44.77
HRDA [76]	TPAMI 23	39.63	38.69	42.21	39.18
SHADE* [64]	IJCV 24	46.66	43.66	45.50	45.27
DGInStyle [45]	ECCV 24	46.89	42.81	50.19	46.63
Ours	-	50.18	43.45	50.72	48.13

5.2 Single-Domain Semantic Segmentation (SDG-SS)

5.2.1 Experimental Setup

Datasets Following established SDG-SS protocols [27], we utilize GTA [77] as our source dataset, comprising 24,966 synthetic images. To evaluate cross-domain performance, three real-world autonomous driving datasets are employed. Cityscapes (CS) [66] offers 500 German urban validation images. BDD100K (BDD) [65] provides 1,000 U.S. cityscape validation samples. Mapillary Vistas (MV) [78] contains 2,000 globally sourced street images showcasing diverse environmental conditions. All experiments focus on 19

Table 5 Component-wise ablation studies on the SDG-OD benchmark.

DFDR		MDSF	MIC	Source	Target			
$\mathcal{L}_{\text{align}}$	$\mathcal{L}_{\text{rea.}}$	\mathcal{L}_{adv}		D-Clear	N-Sunny	D-Rainy	N-Rainy	D-Foggy
				50.2	31.2	26.0	12.1	32.0
	✓			56.0	40.5	32.8	14.2	35.1
✓	✓			57.0	40.5	32.7	14.9	35.4
		✓		54.1	35.8	31.4	13.2	36.2
✓	✓	✓		<u>57.5</u>	40.5	<u>34.5</u>	<u>16.2</u>	<u>37.5</u>
			✓	57.2	39.9	32.2	15.2	36.6
✓	✓	✓	✓	57.6	<u>40.2</u>	39.8	20.2	38.6

overlapping semantic categories common to these datasets.

Implementation and Evaluation Adhering to standard practices in SDG-SS, we evaluate our method using the DeepLabV2 [79] architecture with a ResNet-101 backbone, pre-trained on ImageNet [80]. For virtual domain generation, we adopt the Stable Diffusion 1.5-based pipeline for semantic segmentation introduced by Jia et al. [45], creating 6,000 virtual images with diverse weather conditions to serve as our pseudo-target domain. Based on the multi-resolution self-training strategy and training parameters suggested in MIC, we set the AdamW learning rates for the encoder and decoder at 6×10^{-5} and 6×10^{-4} , respectively. Under the aligned SDG framework detailed in [64], the model is trained for 40,000 iterations with a batch size of 2. Training and testing use 19 shared semantic categories, with the mean Intersection over Union (mIoU) over the 19 classes as the primary evaluation metric on the target datasets.

5.2.2 Comparison with State-of-the-Art Methods

Table 4 compares DRDF against state-of-the-art SDG-SS methods, including classical techniques (IBN-Net [59], ISW [61]) and recent advances (SHADE [64], DGInStyle [45]). Using a ResNet-101 backbone trained on GTA, DRDF attains a 48.13% average mIoU across three real-world target datasets, surpassing existing techniques by 1.5%. Importantly, DRDF upholds strict SDG constraints, unlike methods requiring extra real-world data (marked with *) or unrealistic checkpoint selection (e.g., FSDR [72]). Despite this, DRDF achieves top performance on all datasets: 50.18% on Cityscapes, 43.45% on BDD100K, and

50.72% on Mapillary. It outperforms SHADE [64] and WEDGE [75] by 2.86% and 3.33% in average mIoU, respectively. This validates our innovation of combining virtual domain reassembly and soft fusion strategies to learn domain-invariant representations, advancing SDG-SS.

5.3 Ablation Study

5.3.1 Component Contributions

Table 5 summarizes the performance impact of DFDR and MDSF components. Experiments used Faster R-CNN as the baseline, with the Daytime-Clear (D-clear) domain as the source, evaluating mAP across four target domains.

The first row of Table 5 gives the baseline results. The second row concerns the feature reassembly loss. By ablating only the feature reassembly loss, we achieve a substantial 5.8% improvement in performance on the source domain, with significant gains in the target domains, specifically a 9.3% increase in the Night-Sunny(N-Sunny) scenario. This indicates that an entropy difference-driven mechanism effectively selects robust and discriminative feature channels under different lighting conditions.

Adding alignment loss (third row) further elevates performance to 57.0% in the source domain, with an extra 0.7% gain in Night-Rainy (N-Rainy) conditions. This demonstrates feature alignment reduces structural domain differences, particularly under extreme low-light settings. The domain adversarial loss of MDSF (third row) alone also shows strong performance, especially in Daytime-Foggy(D-Foggy) scenarios (+4.2%). This highlights the value of adversarial training in constructing continuous domain spaces for invariant feature learning.

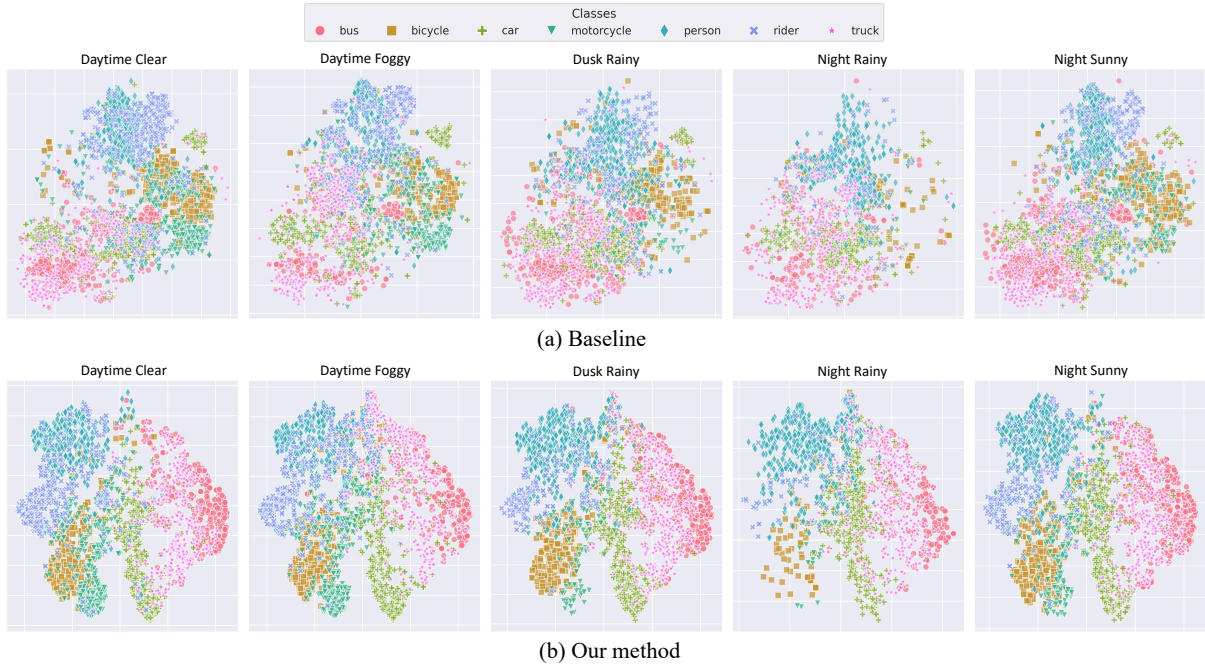


Fig. 7 T-SNE visualization comparing the feature distributions of the Baseline and our method for SDG-OD. Subfigures (a) and (b) depict the class feature distributions across five different domains for the Baseline and our method, respectively

The fourth row of Table 5 shows that the adversarial loss afforded by MDSF alone provides a fair amount of performance gain, with the Daytime-Foggy scenario achieving a +4.2% increase. It thereby validates the formulation of a continuous domain transformation space in which the model is adversarially trained to learn domain-invariant representations. Joined together, DFDR and MDSF provide the best performance across all domains. This synergy arises from complementary roles: DFDR isolates domain-invariant features, while MDSF smooths cross-domain transitions through feature fusion.

Moreover, leveraging pseudo-target domain data for MIC-based domain adaptation inherently improves performance (57.2% on the source domain). Integrating DFDR and MDSF further enhances results, particularly in Dusk-Rainy and Night-Rainy scenarios, with additional gains of 7.6% and 4.0%, respectively. This confirms the compatibility of our joint optimization framework with existing UDA techniques.

Table 6 Ablation study exploring the impact of applying DFDR at different stages of the ResNet-101 Backbone

Method	DS	NS	DR	NR	DF
Baseline	50.2	31.2	26.0	12.1	32.0
+ DFDR (res1)	56.0	39.5	38.8	18.7	37.1
+ DFDR (res2)	57.0	39.8	39.4	18.2	36.2
+ DFDR (res3)	57.1	40.5	37.5	17.2	37.5
+ DFDR (res123)	57.6	40.2	39.8	20.2	38.6
+ DFDR (res1234)	53.6	35.6	34.1	14.4	35.6

5.3.2 Analysis of Network Layer Impact

Table 6 details the impact of applying DFDR to different ResNet-101 residual blocks (res1-4), revealing three key findings: 1) Layer-Specific Sensitivity: Applying DFDR at a single layer yields significant gains, with different layers showing selective sensitivity to specific domain shifts. The res1 configuration (shallow features) notably improves the Night-Rainy (NR) scenario (+6.6%), res2 excels in Dusk-Rainy (DR) (+13.4%), while res3 boosts Night-Sunny (NS) and Daytime-Foggy (DF) by 9.3% and 5.5%, respectively. This suggests that features captured at different levels exhibit varying sensitivities to different types of

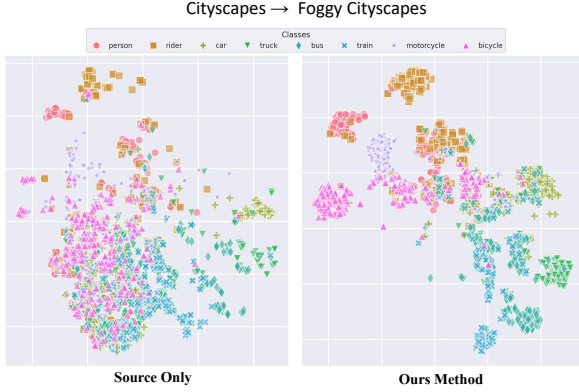


Fig. 8 T-SNE visualization of feature embeddings in object detection domain adaptation, comparing source-only training with our proposed domain adaptation approach.

domain shifts. 2) Multi-Layer Complementarity: Applying DFDR to the first three residual blocks (res123) achieves optimal performance, improving the source domain by 7.4% and target domains by an average of 10.9%. This multi-level configuration enables simultaneous feature decoupling and reorganization at varying abstraction levels: shallow layers handle textures and low-level features, mid-layers process object structure and contours, collectively building a hierarchical domain-invariant representation. 3) Deep Layer Applicability Limitations: Extending DFDR to all layers (res1234) significantly degrades performance, echoing observations by Zhou et al. [33]. This is primarily because res4, located deep within the network, possesses highly semantic feature representations tightly coupled with category labels. Applying feature decoupling at this level disrupts the model’s ability to capture high-level semantic information, reducing discrimination.

5.3.3 Synergistic Effects with Different UDA Methods

To validate the DRSF-UDA integration paradigm, Table 7 compares performance when combined with three representative UDA methods.

SADA [6], which addresses image-level and instance-level domain shifts, performs best in rainy scenarios when integrated with our framework. This suggests that the synthetic pseudo-target domain successfully captures key rainy

Table 7 Ablation study on the effect of UDA methods.

Method	DS	NS	DR	NR	DF
Baseline	50.2	31.2	26.0	12.1	32.0
+ SADA	<u>57.6</u>	39.3	40.8	20.7	<u>38.5</u>
+ HRDA	57.4	<u>39.6</u>	<u>40.1</u>	18.7	37.5
+ MIC	57.7	40.2	39.8	<u>20.2</u>	38.6

visual characteristics, enabling SADA’s scale-aware self-adaptation mechanism to effectively learn target representations under complex conditions.

HRDA [81], leveraging multi-resolution training to combine high-resolution details with low-resolution context, excels in the Night-Sunny scenario. This stems from the pseudo-target domain’s preservation of night scene structural information, allowing HRDA’s multi-resolution strategy to extract rich contextual cues.

MIC, learning spatial contextual relationships through masked image consistency, performs exceptionally well in the Daytime-Foggy scenario. MIC’s mask prediction mechanism can learn deep spatial dependencies from the pseudo-target domain, effectively overcoming limitations in fog scene simulation.

Performance variations among UDA methods across scenarios reflect fluctuations in pseudo-target domain generation quality. In lighting change scenarios (e.g., Night-Sunny), the three methods perform similarly. However, in multi-factor degradation scenarios (e.g., Night-Rainy), performance differences widen, indicating limitations in the pseudo-target domain’s ability to simulate complex degradation, and varying sensitivities of UDA methods to pseudo-target domain quality. These results thoroughly validate the effectiveness of our proposed “pseudo-target domain-driven domain adaptation” paradigm. By generating high-quality pseudo-target domains and integrating advanced UDA techniques, we achieve superior generalization performance without relying on real target domain data.

5.3.4 Ablation Study on Synthetic Domains

In this section we systematically analyzed how different pseudo-target domain combinations affect model performance. Table 8 illustrates the impact

Table 8 Ablation study on the effect of pseudo target domain.

Method	DS	NS	DR	NR	DF
Baseline	50.2	31.2	26.0	12.1	32.0
+ pseudo DS	55.6	39.6	36.9	18.3	37.3
+ pseudo NS	55.0	40.2	<u>37.0</u>	18.5	36.5
+ pseudo DR	55.3	40.0	<u>36.5</u>	16.2	35.5
+ pseudo NR	54.1	38.1	36.6	<u>19.8</u>	35.4
+ pseudo DF	54.5	39.2	36.0	18.3	<u>38.1</u>
+ all	57.7	40.2	39.8	20.2	38.6

of five pseudo-target domains across five test domains, revealing several key insights:

1) Target Correspondence Effect: Each pseudo-target domain consistently performs best on its corresponding real target domain, confirming our generation strategy’s precision. The pseudo-NS domain achieves 40.2% mAP on the real NS test domain, pseudo-NR reaches 19.8% on the real NR test domain, and pseudo-DF attains 38.1% detection accuracy on the real DF test domain. Notably, even the pseudo-source domain (DS) generation boosts source domain performance by 5.4%, demonstrating the internal regularization benefits of feature decoupling and reorganization.

2) Cross-domain Transfer Ability: Pseudo-target domains not only enhance performance on their corresponding test domains but also improve results across other test scenarios. For instance, the pseudo-NS domain dramatically boosts the DR test domain by 11 percentage points, while the pseudo-DS domain improves the NR test domain by 6.2 percentage points. This indicates successful capture of domain-invariant features that transfer across different environmental conditions.

3) Multi-domain Synergistic Effect: The “+ all” configuration (utilizing all pseudo-target domains) achieves optimal performance across all test scenarios, improving the source domain from 50.2% to 57.7% and target domains by an average of 10.5 percentage points. This multi-domain joint training exhibits significant synergistic effects compared to any single pseudo-target domain. On the DR test domain, for example, the full pseudo-domain configuration (39.8%) outperforms the best single pseudo-domain (37.0%) by 2.8 percentage points. These results validate our core hypothesis that different pseudo-target domains capture complementary aspects of environmental variations, collectively building a more

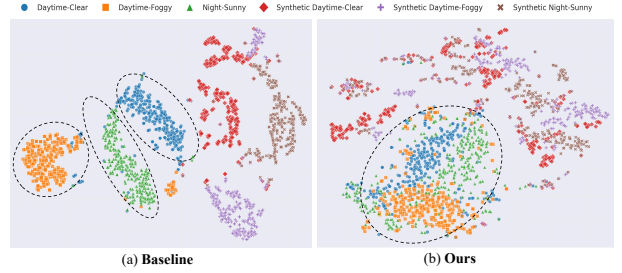


Fig. 9 t-SNE visualization of domain features: (a) Baseline models show clear separation between real and synthetic domains, indicating significant differences. (b) DRSF achieves better fusion between the real source domain (Daytime-Clear) and target domains (Daytime-Foggy and Night-Sunny), demonstrating effective domain-invariant representations.

comprehensive domain generalization representation space.

4) Source Domain Feedback Mechanism: The all-domains configuration not only enhances target domain performance but also elevates source domain performance to 57.7%. This phenomenon indicates that domain-invariant features learned through diverse pseudo-target domains benefit source domain representations, improving performance across all scenarios and eliminating the typical source-target performance trade-off in domain generalization.

These findings comprehensively validate our approach’s effectiveness. By generating diverse pseudo-target domains and integrating feature decoupling with domain fusion techniques, we significantly enhance cross-domain generalization without requiring real target domain data.

5.4 Further evaluation

5.4.1 Comparison with Domain Adaptation Methods

To evaluate the proposed “DRSF-UDA integration” framework from Section 3.4.3, we conducted comparative experiments with conventional unsupervised domain adaptation (UDA) techniques across two standard cross-domain scenarios. Unlike traditional UDA approaches requiring access to target-domain samples, our investigation explores substituting or supplementing real target-domain data with synthetically generated pseudo-domain data.

Table 9 Per-class Results from Daytime Clear to Night Sunny. The results of DAOD methods are from [62].

Method	target	Bus	Bike	Car	Motor	Person	Rider	Truck	mAP
SO[2]	✗	37.7	30.6	49.5	15.4	31.5	28.6	40.8	33.5
DAF [82]	✓	36.2	29.1	49.3	16.0	33.1	29.3	40.2	33.3
CT [83]	✓	34.1	22.1	46.4	12.8	26.5	19.8	31.5	27.6
SCL [84]	✓	27.1	18.6	45.9	11.6	24.0	19.0	32.3	25.5
SW [58]	✓	34.2	23.6	48.0	13.4	26.4	23.7	37.5	29.5
ICCR [85]	✓	36.1	23.2	48.9	15.5	29.1	23.8	39.4	30.9
HTCN [86]	✓	30.5	17.6	44.7	11.0	22.9	20.6	31.3	25.5
VDD [87]	✓	35.4	29.6	49.8	14.5	31.3	28.0	39.9	32.6
Ours	✗	41.9	38.3	65.2	16.4	43.9	30.7	45.3	40.2
Ours	✓	38.6	40.2	63.2	20.4	44.6	29.5	40.3	39.5

Table 10 Comparison with UDA methods for adapting from Cityscapes to FoggyCityscapes (clear to foggy).

Methods	Bus	Bicycle	Car	Motor	Person	Rider	Train	Truck	mAP
SCDA [88]	39.0	33.6	48.5	28.0	33.5	38.0	23.3	26.5	33.8
DA-Faster [82]	49.8	39.0	53.0	28.9	35.7	45.2	45.4	30.9	41.0
GPA [89]	45.7	38.7	54.1	32.4	32.9	46.7	41.1	24.7	39.5
RPN-PR [90]	43.6	36.8	50.5	29.7	33.3	45.6	42.0	30.4	39.0
UaDAN [91]	49.4	38.9	53.6	32.3	36.5	46.1	42.7	28.9	41.1
AdvGRL [67]	51.2	39.1	54.3	31.6	36.5	46.7	48.7	30.3	42.3
D-adapt [7]	42.8	42.4	56.8	35.2	42.8	48.4	37.4	31.5	42.2
Ours	54.7	41.0	59.3	33.8	45.7	48.9	27.8	34.8	43.5

Daytime-to-Night Adaptation As shown in Table 9, our method achieves a 40.2% mAP without using any real nighttime target-domain data (denoted by “✗”), outperforming all UDA baselines that rely on real target-domain data. The performance gains are particularly pronounced in “Car” (15.4% improvement) and “Person” (12.6% improvement) categories over the best UDA method. Counterintuitively, incorporating real target-domain data (marked “✓”) resulted in a slight performance drop to 39.5% mAP. This unexpected trend suggests that noise and distribution biases in real target-domain samples may disrupt the domain-invariant feature learning from pseudo data. Notable degradation occurred in “Bus” (-3.3%) and “Truck” (-5.0%) categories, likely due to uneven nighttime lighting affecting large vehicle detection.

Sunny-to-Foggy Adaptation Table 10 demonstrates our method’s 43.5% mAP performance in foggy cityscape adaptation, surpassing competitive methods like AdvGRL and UaDAN. Five out of eight categories achieved state-of-the-art results, highlighting the DRSF framework’s robustness against fog-induced visual degradation.

Limitations were observed in “Train” category performance, attributable to sparse and morphologically diverse train samples challenging the feature decoupling strategy for large-rare objects. “Motor” category underperformance likely stems from fog-induced contour ambiguity hindering structural feature recovery. Despite these challenges, the results validate DRSF’s dual efficacy: as a standalone domain generalization method and as an enhancement module for UDA approaches. This enables superior performance with minimal reliance on real target-domain data, underscoring the practical utility of our proposed framework.

5.4.2 Visual Analysis of Discriminative Model Features

To intuitively demonstrate DRSF’s improvements in feature representation, we visualized feature distributions across different domains using t-SNE, with detector-derived exemplar features representing category distributions. Fig. 7 contrasts the feature spaces of baseline and DRSF models under the SDG-OD setting. The visualization highlights key differences: the baseline

Table 11 Performance on the Adverse-Weather dataset and computational complexity comparison.

Model	Complexity		Performance	
	Params	GFLOPs	Source	Target
ResNet-101	9.60M	24.67	50.2	25.3
+ DRSF Δ	9.97M	26.76	57.5	32.4
	+3.8%	+8.4%	+14.5%	+28.1%
+ MIC Δ	13.45M	48.28	57.7	34.7
	+40.1%	+95.7%	+14.9%	+37.2%

model’s feature distribution exhibits distinct separation between source and target domains, with weak intra-class clustering. In contrast, DRSF achieves superior cross-domain alignment, maintaining the aggregation of same-category samples across domains. Especially in the sunny-to-foggy domain adaptation task (Fig. 8), the baseline model displays blurred inter-class boundaries and significant feature overlap, whereas DRSF effectively enhances feature discriminability, resulting in clear category boundaries. These visual results directly validate that DRSF successfully learns cross-domain shared discriminative representations while mitigating domain-specific interference.

5.4.3 Domain Feature Distribution Visualization

This section presents an in-depth visualization analysis of feature representations learned by the DRSF framework. Fig. 9 illustrates feature distributions extracted from the real source domain, real target domains, and synthetic pseudo-target domains.

Fig. 9(a) reveals that the baseline model (Faster R-CNN) forms distinct domain clusters in the feature space: the three real domains—Daytime-Clear (blue circles), Daytime-Foggy (orange squares), and Night-Sunny (green triangles)—form mutually independent clusters, indicating a substantial domain shift. Notably, the synthetic pseudo-target domain data also exhibits a distribution distinct from the real domains, suggesting that models lacking feature decoupling and reassembly cannot effectively leverage synthetic data to bridge domain gaps. Conversely, Fig. 9(b) showcases the feature distribution learned by DRSF, presenting a markedly different pattern where the feature distributions of the

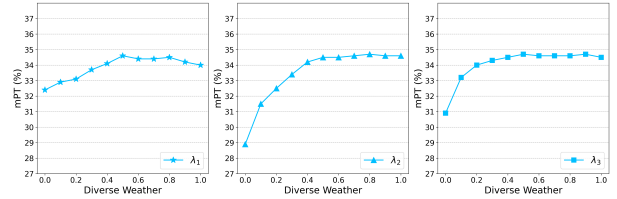


Fig. 10 Sensitivity analysis to evaluate the impact of hyper-parameter λ_1 , λ_2 and λ_3 on the performance of the SDG-OD task.

three real domains exhibit high overlap, domain boundaries become less defined, and a more unified feature space emerges. This feature alignment directly confirms DRSF’s capability for domain-invariant representation learning. In particular, the features of the real source domain (blue) and the two real target domains (orange and green) are closely integrated, indicating that DRSF successfully constructs a cross-domain shared semantic space, effectively overcoming superficial feature differences induced by environmental variations.

5.4.4 Complexity Analysis

To assess the practicality of the DRSF framework, we conducted a complexity analysis, as detailed in Table 11. Compared to the ResNet-101 baseline, DRSF achieves significant performance gains with only a 3.8% increase in parameters and an 8.4% increase in computational complexity. DRSF’s efficiency stems primarily from its lightweight feature decoupling and reassembly design: by employing instance normalization and channel attention mechanisms, we avoid complex feature transformations or a large number of additional parameters, focusing instead on exploiting and recombining the latent value of existing features. While combining DRSF with the MIC method further improves performance, it also substantially increases computational complexity. This increase is mainly attributed to MIC’s masked image processing and consistency learning mechanisms, which necessitate maintaining additional teacher networks and mask prediction modules. The complexity analysis demonstrates that DRSF maintains remarkably low computational overhead while delivering substantial performance improvements. Furthermore, its compatibility with UDA methods underscores the flexibility of our method’s deployment.

5.4.5 Hyperparameter Sensitivity Analysis

We investigated the influence of three key hyperparameters controlling the feature alignment loss (λ_1), feature reassembly loss (λ_2), and domain adversarial loss (λ_3). Fig. 10 illustrates how the target domain mPT varies with these parameters.

For λ_1 , performance increases steadily as the weight grows from 0 to 0.5, but plateaus thereafter with marginal declines at higher values. This suggests moderate alignment effectively reduces domain structural differences without over-suppressing domain-specific feature learning. The λ_2 parameter shows the strongest impact, demonstrating nearly linear performance improvement across its range, underscoring the critical role of entropy-driven feature reassembly. The λ_3 parameter exhibits a “rapid saturation” pattern: performance jumps sharply from 30.9% to 34.7% as λ_3 reaches 0.5, then stabilizes. This indicates sufficient adversarial strength enables the soft fusion mechanism to create a smooth feature transition space across pseudo-target domains.

Based on this analysis, we recommend optimal settings of $\lambda_1 = 0.5$, $\lambda_2 = 0.8$, and $\lambda_3 = 0.5$, which achieve the best trade-off between performance enhancement and model stability. The results also highlight the importance of balancing adversarial learning intensity with domain adaptation objectives.

6 Conclusion and Discussion

This work addresses the critical challenge in SDG where synthetic data generated by LDMs often degrades model performance due to domain distribution discrepancies. We propose DRFSF, a novel training framework that mitigates this issue through a feature-level domain reassembly and soft-fusion strategy. Our extensive experiments demonstrate DRFSF’s effectiveness in improving cross-domain performance with minimal computational overhead. Moreover, DRFSF’s plug-and-play architecture enables seamless integration into existing pipelines, including extensions to unsupervised domain adaptation paradigms.

Limitations include current pseudo-domain generation’s struggle with complex multi-degradation scenarios, which we propose to address through closed-loop optimization systems

integrating model feedback. Future work should explore extending DRFSF to multi-modal tasks such as instance segmentation [92], and medical imaging [93]. Additionally, combining DRFSF with visual foundation models like [94] could leverage pre-trained model priors to further enhance generalization.

DRFSF establishes a general approach to SDG by systematically addressing feature distribution bias and domain space coverage. Its plug-and-play design bridges the gap between synthetic data utilization and real-world domain adaptation needs, offering a practical solution for data-scarce environments while maintaining computational efficiency. This work not only advances SDG methodology but also provides a generalizable paradigm for DG research in open-world vision tasks.

Data Availability

The generated data used during the current study are available as follows: Object detection: Semantic segmentation:

The datasets analysed during the current study are available as follows: Diverse Weather [62]: <https://github.com/AmingWu/Single-DGOD> GTAV [77]: https://download.visinf.tu-darmstadt.de/data/from_games/ CityScapes [66]: <https://www.cityscapes-dataset.com/> BDD100K [65]: <https://bdd-data.berkeley.edu/> Mapillary [78]: <https://www.mapillary.com/dataset/vistas>.

References

- [1] LeCun, Y., Bengio, Y., Hinton, G.: Deep learning. *nature* **521**(7553), 436–444 (2015)
- [2] Ren, S., He, K., Girshick, R., Sun, J.: Faster r-cnn: Towards real-time object detection with region proposal networks. *NeurIPS* **28** (2015)
- [3] Wang, W., Li, H., Wang, C., Huang, C., Ding, Z., Nie, F., Cao, X.: Deep label propagation with nuclear norm maximization for visual domain adaptation. *TIP* (2025)
- [4] Zhou, K., Yang, Y., Qiao, Y., Xiang, T.: Domain adaptive ensemble learning. *TIP* **30**, 8008–8018 (2021)

- [5] Ben-David, S., Blitzer, J., Crammer, K., Kulesza, A., Pereira, F., Vaughan, J.W.: A theory of learning from different domains. *Machine learning* **79**, 151–175 (2010)
- [6] Chen, Y., Wang, H., Li, W., Sakaridis, C., Dai, D., Van Gool, L.: Scale-aware domain adaptive faster r-cnn. *IJCV* **129**(7), 2223–2243 (2021)
- [7] Jiang, J., Chen, B., Wang, J., Long, M.: Decoupled adaptation for cross-domain object detection. In: *The International Conference on Learning Representations (ICLR)* (2022)
- [8] Bellitto, G., Proietto Salanitri, F., Palazzo, S., Rundo, F., Giordano, D., Spampinato, C.: Hierarchical domain-adapted feature learning for video saliency prediction. *IJCV* **129**, 3216–3232 (2021)
- [9] Du, D., Chen, J., Li, Y., Ma, K., Wu, G., Zheng, Y., Wang, L.: Cross-domain gated learning for domain generalization. *IJCV* **130**(11), 2842–2857 (2022)
- [10] Zhou, K., Loy, C.C., Liu, Z.: Semi-supervised domain generalization with stochastic stylematch. *IJCV* **131**(9), 2377–2387 (2023)
- [11] Zhao, Y., Zhong, Z., Zhao, N., Sebe, N., Lee, G.H.: Style-hallucinated dual consistency learning: A unified framework for visual domain generalization. *IJCV* **132**(3), 837–853 (2024)
- [12] Zhou, K., Liu, Z., Qiao, Y., Xiang, T., Loy, C.C.: Domain generalization: A survey. *TPAMI* **45**(4), 4396–4415 (2022)
- [13] Yuan, J., Ma, X., Chen, D., Kuang, K., Wu, F., Lin, L.: Domain-specific bias filtering for single labeled domain generalization. *IJCV* **131**(2), 552–571 (2023)
- [14] Su, Z., Yao, K., Yang, X., Huang, K., Wang, Q., Sun, J.: Rethinking data augmentation for single-source domain generalization in medical image segmentation. In: *AAAI*, vol. 37, pp. 2366–2374 (2023)
- [15] Zheng, G., Huai, M., Zhang, A.: Advst: Revisiting data augmentations for single domain generalization. In: *AAAI*, vol. 38, pp. 21832–21840 (2024)
- [16] Termöhlen, J.-A., Bartels, T., Fingscheidt, T.: A re-parameterized vision transformer (revt) for domain-generalized semantic segmentation. In: *ICCV*, pp. 4376–4385 (2023)
- [17] Liu, Y., Zhou, S., Liu, X., Hao, C., Fan, B., Tian, J.: Unbiased faster r-cnn for single-source domain generalized object detection. In: *CVPR*, pp. 28838–28847 (2024)
- [18] Schuhmann, C., Beaumont, R., Vencu, R., Gordon, C., Wightman, R., Cherti, M., Coombes, T., Katta, A., Mullis, C., Wortsman, M., *et al.*: Laion-5b: An open large-scale dataset for training next generation image-text models. *NeurIPS* **35**, 25278–25294 (2022)
- [19] Vedit, V., Engilberge, M., Salzmann, M.: CLIP the gap: A single domain generalization approach for object detection. In: *CVPR*, pp. 3219–3229 (2023)
- [20] Vapnik, V.: Principles of risk minimization for learning theory. *NeurIPS* **4** (1991)
- [21] Yang, X., Chang, T., Zhang, T., Wang, S., Hong, R., Wang, M.: Learning hierarchical visual transformation for domain generalizable visual matching and recognition. *IJCV* **132**(11), 4823–4849 (2024)
- [22] Zhao, S., Li, B., Xu, P., Yue, X., Ding, G., Keutzer, K.: Madan: Multi-source adversarial domain aggregation network for domain adaptation. *IJCV* **129**(8), 2399–2424 (2021)
- [23] Munir, M.A., Khan, M.H., Sarfraz, M.S., Ali, M.: Domain adaptive object detection via balancing between self-training and adversarial learning. *TPAMI* (2023)
- [24] Qu, X., Zhang, H., Zhu, L., Nie, L., Liu, L.: Aamt: Adversarial attack-driven mutual teaching for source-free domain-adaptive person reidentification. *TMM* (2024)

- [25] Wang, W., Li, H., Ding, Z., Nie, F., Chen, J., Dong, X., Wang, Z.: Rethinking maximum mean discrepancy for visual domain adaptation. *TNNLS* **34**(1), 264–277 (2021)
- [26] Li, P., Li, D., Li, W., Gong, S., Fu, Y., Hospedales, T.M.: A simple feature augmentation for domain generalization. In: *ICCV*, pp. 8886–8895 (2021)
- [27] Wang, M., Yuan, J., Qian, Q., Wang, Z., Li, H.: Semantic data augmentation based distance metric learning for domain generalization. In: *ACM MM*, pp. 3214–3223 (2022)
- [28] Zeng, Q., Wang, W., Zhou, F., Ling, C., Wang, B.: Foresee what you will learn: data augmentation for domain generalization in non-stationary environment. In: *AAAI*, vol. 37, pp. 11147–11155 (2023)
- [29] Li, D., Yang, Y., Song, Y.-Z., Hospedales, T.: Learning to generalize: Meta-learning for domain generalization. In: *AAAI*, vol. 32 (2018)
- [30] Shu, Y., Cao, Z., Wang, C., Wang, J., Long, M.: Open domain generalization with domain-augmented meta-learning. In: *CVPR*, pp. 9624–9633 (2021)
- [31] Chen, C., Li, J., Han, X., Liu, X., Yu, Y.: Compound domain generalization via meta-knowledge encoding. In: *CVPR*, pp. 7119–7129 (2022)
- [32] Khoei, A.G., Yu, Y., Feldt, R.: Domain generalization through meta-learning: A survey. *Artificial Intelligence Review* **57**(10), 285 (2024)
- [33] Zhou, K., Yang, Y., Qiao, Y., Xiang, T.: Mixstyle neural networks for domain generalization and adaptation. *IJCV* **132**(3), 822–836 (2024)
- [34] Qiao, F., Zhao, L., Peng, X.: Learning to learn single domain generalization. In: *CVPR*, pp. 12556–12565 (2020)
- [35] Wang, Z., Luo, Y., Qiu, R., Huang, Z., Baktashmotlagh, M.: Learning to diversify for single domain generalization. In: *ICCV*, pp. 834–843 (2021)
- [36] Carlucci, F.M., D’Innocente, A., Bucci, S., Caputo, B., Tommasi, T.: Domain generalization by solving jigsaw puzzles. In: *CVPR*, pp. 2229–2238 (2019)
- [37] Chen, T., Baktashmotlagh, M., Wang, Z., Salzmann, M.: Center-aware adversarial augmentation for single domain generalization. In: *WACV*, pp. 4157–4165 (2023)
- [38] Lee, W., Hong, D., Lim, H., Myung, H.: Object-aware domain generalization for object detection. In: *AAAI*, vol. 38, pp. 2947–2955 (2024)
- [39] Vidit, V., Engilberge, M., Salzmann, M.: Clip the gap: A single domain generalization approach for object detection. In: *CVPR*, pp. 3219–3229 (2023)
- [40] Radford, A., Kim, J.W., Hallacy, C., Ramesh, A., Goh, G., Agarwal, S., Sastry, G., Askell, A., Mishkin, P., Clark, J., Krueger, G., Sutskever, I.: Learning transferable visual models from natural language supervision. In: *ICML*, vol. 139, pp. 8748–8763 (2021)
- [41] Rombach, R., Blattmann, A., Lorenz, D., Esser, P., Ommer, B.: High-resolution image synthesis with latent diffusion models. In: *CVPR*, pp. 10684–10695 (2022)
- [42] Danish, M.S., Khan, M.H., Munir, M.A., Sarfraz, M.S., Ali, M.: Improving single domain-generalized object detection: A focus on diversification and alignment. In: *CVPR*, pp. 17732–17742 (2024)
- [43] Li, D., Wu, A., Wang, Y., Han, Y.: Prompt-driven dynamic object-centric learning for single domain generalization. In: *CVPR*, pp. 17606–17615 (2024)
- [44] Wang, X., Darrell, T., Rambhatla, S.S., Girdhar, R., Misra, I.: Instancediffusion: Instance-level control for image generation. In: *CVPR*, pp. 6232–6242 (2024)
- [45] Jia, Y., Hoyer, L., Huang, S., Wang, T.,

- Van Gool, L., Schindler, K., Obukhov, A.: Dginstyle: Domain-generalizable semantic segmentation with image diffusion models and stylized semantic control. In: ECCV, pp. 91–109 (2024). Springer
- [46] Goodfellow, I., Pouget-Abadie, J., Mirza, M., Xu, B., Warde-Farley, D., Ozair, S., Courville, A., Bengio, Y.: Generative adversarial networks. *Communications of the ACM* **63**(11), 139–144 (2020)
- [47] Kingma, D.P., Welling, M.: Auto-Encoding Variational Bayes (2022). <https://arxiv.org/abs/1312.6114>
- [48] Li, H., Yang, X., Wang, M., Lan, L., Liang, K., Liu, X., Li, K.: Object style diffusion for generalized object detection in urban scene. arXiv preprint arXiv:2412.13815 (2024)
- [49] Ulyanov, D., Vedaldi, A., Lempitsky, V.: Instance normalization: The missing ingredient for fast stylization. arXiv preprint arXiv:1607.08022 (2016)
- [50] Huang, X., Belongie, S.: Arbitrary style transfer in real-time with adaptive instance normalization. In: ICCV, pp. 1501–1510 (2017)
- [51] Li, Y., Wang, N., Liu, J., Hou, X.: Demystifying neural style transfer. arXiv preprint arXiv:1701.01036 (2017)
- [52] Gretton, A., Borgwardt, K.M., Rasch, M.J., Schölkopf, B., Smola, A.: A kernel two-sample test. *JMLR* **13**(1), 723–773 (2012)
- [53] Hu, J., Shen, L., Sun, G.: Squeeze-and-excitation networks. In: CVPR, pp. 7132–7141 (2018)
- [54] Lee, H., Kim, H.-E., Nam, H.: Srm: A style-based recalibration module for convolutional neural networks. In: ICCV, pp. 1854–1862 (2019)
- [55] Xu, M., Zhang, J., Ni, B., Li, T., Wang, C., Tian, Q., Zhang, W.: Adversarial domain adaptation with domain mixup. In: AAI, vol. 34, pp. 6502–6509 (2020)
- [56] Ganin, Y., Lempitsky, V.: Unsupervised domain adaptation by backpropagation. In: ICML, pp. 1180–1189 (2015). PMLR
- [57] Lin, T.-Y., Goyal, P., Girshick, R., He, K., Dollár, P.: Focal loss for dense object detection. In: ICCV, pp. 2980–2988 (2017)
- [58] Pan, X., Zhan, X., Shi, J., Tang, X., Luo, P.: Switchable whitening for deep representation learning. In: ICCV, pp. 1863–1871 (2019)
- [59] Pan, X., Luo, P., Shi, J., Tang, X.: Two at once: Enhancing learning and generalization capacities via ibn-net. In: ECCV, pp. 464–479 (2018)
- [60] Huang, L., Zhou, Y., Zhu, F., Liu, L., Shao, L.: Iterative normalization: Beyond standardization towards efficient whitening. In: CVPR, pp. 4874–4883 (2019)
- [61] Choi, S., Jung, S., Yun, H., Kim, J.T., Kim, S., Choo, J.: Robustnet: Improving domain generalization in urban-scene segmentation via instance selective whitening. In: CVPR, pp. 11580–11590 (2021)
- [62] Wu, A., Deng, C.: Single-domain generalized object detection in urban scene via cyclic-disentangled self-distillation. In: CVPR, pp. 847–856 (2022)
- [63] Rao, Z., Guo, J., Tang, L., Huang, Y., Ding, X., Guo, S.: Srcd: Semantic reasoning with compound domains for single-domain generalized object detection. TNNLS (2024)
- [64] Zhao, Y., Zhong, Z., Zhao, N., Sebe, N., Lee, G.H.: Style-hallucinated dual consistency learning: A unified framework for visual domain generalization. *IJCV* **132**(3), 837–853 (2024)
- [65] Yu, F., Chen, H., Wang, X., Xian, W., Chen, Y., Liu, F., Madhavan, V., Darrell, T.: Bdd100k: A diverse driving dataset for heterogeneous multitask learning. In: CVPR, pp. 2636–2645 (2020)
- [66] Cordts, M., Omran, M., Ramos, S., Rehfeld, T., Enzweiler, M., Benenson, R., Franke, U.,

- Roth, S., Schiele, B.: The cityscapes dataset for semantic urban scene understanding. In: CVPR, pp. 3213–3223 (2016)
- [67] Li, J., Xu, R., Ma, J., Zou, Q., Ma, J., Yu, H.: Domain adaptive object detection for autonomous driving under foggy weather. In: WACV, pp. 612–622 (2023)
- [68] Hoyer, L., Dai, D., Wang, H., Van Gool, L.: Mic: Masked image consistency for context-enhanced domain adaptation. In: CVPR, pp. 11721–11732 (2023)
- [69] He, K., Zhang, X., Ren, S., Sun, J.: Deep residual learning for image recognition. In: CVPR, pp. 770–778 (2016)
- [70] Peng, D., Lei, Y., Liu, L., Zhang, P., Liu, J.: Global and local texture randomization for synthetic-to-real semantic segmentation. *TIP* **30**, 6594–6608 (2021)
- [71] Peng, D., Lei, Y., Hayat, M., Guo, Y., Li, W.: Semantic-aware domain generalized segmentation. In: CVPR, pp. 2594–2605 (2022)
- [72] Huang, J., Guan, D., Xiao, A., Lu, S.: Fsd: Frequency space domain randomization for domain generalization. In: CVPR, pp. 6891–6902 (2021)
- [73] Zhong, Z., Zhao, Y., Lee, G.H., Sebe, N.: Adversarial style augmentation for domain generalized urban-scene segmentation. *NeurIPS* **35**, 338–350 (2022)
- [74] Lee, S., Seong, H., Lee, S., Kim, E.: Wildnet: Learning domain generalized semantic segmentation from the wild. In: CVPR, pp. 9936–9946 (2022)
- [75] Kim, N., Son, T., Pahk, J., Lan, C., Zeng, W., Kwak, S.: Wedge: web-image assisted domain generalization for semantic segmentation. In: ICRA, pp. 9281–9288 (2023). IEEE
- [76] Hoyer, L., Dai, D., Van Gool, L.: Domain adaptive and generalizable network architectures and training strategies for semantic image segmentation. *TPAMI* **46**(1), 220–235 (2023)
- [77] Ros, G., Sellart, L., Materzynska, J., Vazquez, D., Lopez, A.M.: The synthia dataset: A large collection of synthetic images for semantic segmentation of urban scenes. In: CVPR, pp. 3234–3243 (2016)
- [78] Neuhold, G., Ollmann, T., Rota Bulo, S., Kotschieder, P.: The mapillary vistas dataset for semantic understanding of street scenes. In: ICCV, pp. 4990–4999 (2017)
- [79] Chen, L.-C., Papandreou, G., Kokkinos, I., Murphy, K., Yuille, A.L.: Deeplab: Semantic image segmentation with deep convolutional nets, atrous convolution, and fully connected crfs. *TPAMI* **40**(4), 834–848 (2017)
- [80] Deng, J., Dong, W., Socher, R., Li, L.-J., Li, K., Fei-Fei, L.: Imagenet: A large-scale hierarchical image database. In: 2009 IEEE Conference on Computer Vision and Pattern Recognition, pp. 248–255 (2009). IEEE
- [81] Hoyer, L., Dai, D., Van Gool, L.: Hrda: Context-aware high-resolution domain-adaptive semantic segmentation. In: ECCV, pp. 372–391 (2022). Springer
- [82] Chen, Y., Li, W., Sakaridis, C., Dai, D., Van Gool, L.: Domain adaptive faster r-cnn for object detection in the wild. In: CVPR, pp. 3339–3348 (2018)
- [83] Zhao, G., Li, G., Xu, R., Lin, L.: Collaborative training between region proposal localization and classification for domain adaptive object detection. In: ECCV, pp. 86–102 (2020). Springer
- [84] Shen, Z., Maheshwari, H., Yao, W., Savvides, M.: Scl: Towards accurate domain adaptive object detection via gradient detach based stacked complementary losses. arXiv preprint arXiv:1911.02559 (2019)
- [85] Xu, C.-D., Zhao, X.-R., Jin, X., Wei, X.-S.: Exploring categorical regularization for domain adaptive object detection. In: CVPR, pp. 11724–11733 (2020)
- [86] Chen, C., Zheng, Z., Ding, X., Huang, Y.,

- Dou, Q.: Harmonizing transferability and discriminability for adapting object detectors. In: CVPR, pp. 8869–8878 (2020)
- [87] Wu, A., Liu, R., Han, Y., Zhu, L., Yang, Y.: Vector-decomposed disentanglement for domain-invariant object detection. In: ICCV, pp. 9342–9351 (2021)
- [88] Zhu, X., Pang, J., Yang, C., Shi, J., Lin, D.: Adapting object detectors via selective cross-domain alignment. In: CVPR, pp. 687–696 (2019)
- [89] Xu, M., Wang, H., Ni, B., Tian, Q., Zhang, W.: Cross-domain detection via graph-induced prototype alignment. In: CVPR, pp. 12355–12364 (2020)
- [90] Zhang, Y., Wang, Z., Mao, Y.: Rpn prototype alignment for domain adaptive object detector. In: CVPR, pp. 12425–12434 (2021)
- [91] Guan, D., Huang, J., Xiao, A., Lu, S., Cao, Y.: Uncertainty-aware unsupervised domain adaptation in object detection. TMM **24**, 2502–2514 (2021)
- [92] Li, H., Wang, W., Wang, M., Tan, H., Lan, L., Luo, Z., Liu, X., Li, K.: Stformer: Spatial-temporal-aware transformer for video instance segmentation. TNNLS (2024)
- [93] Zhang, J., Zhang, S., Shen, X., Lukasiewicz, T., Xu, Z.: Multi-condos: Multimodal contrastive domain sharing generative adversarial networks for self-supervised medical image segmentation. IEEE Transactions on Medical Imaging **43**(1), 76–95 (2023)
- [94] Liu, S., Zeng, Z., Ren, T., Li, F., Zhang, H., Yang, J., Jiang, Q., Li, C., Yang, J., Su, H., *et al.*: Grounding dino: Marrying dino with grounded pre-training for open-set object detection. In: ECCV, pp. 38–55 (2024). Springer